doi:10.1016/j.jmb.2005.10.038 J. Mol. Biol. (2005) xx, 1–13

JMB

Available online at www.sciencedirect.com

SCIENCE DIRECT®

ELSEVIER

# Molecular Dynamics Simulations of the Influenza Hemagglutinin Fusion Peptide in Micelles and Bilayers: Conformational Analysis of Peptide and Lipids

**Patrick Lagüe[1]*, Benoît Roux[2] and Richard W. Pastor[1]**

[1]*Laboratory of Biophysics Center for Biologics Evaluation and Research, FDA, 1401 Rockville Pike, Rockville, MD 20852-1448, USA*

[2]*Department of Biochemistry (Box 63), Weill Medical College of Cornell University, 1300 York Avenue, New York, NY 10021 USA*

**Corresponding author*

Molecular dynamics simulations of the influenza hemagglutinin fusion peptide in two differently sized dodecylphosphocholine micelles and a palmitoyl oleoyl phosphatidylcholine bilayer were generated to analyze the influence of the environment. Four independent trajectories (5 ns each for the bilayer, and 2 ns each for the micelles) were generated for each system. The peptide lies at the surface of the micelles, while its N-terminal region inserts deeply in the bilayer. This leads to a substantial increase of the solvation and rigidity of the peptide in micelles as compared to the bilayer. The average structures, nevertheless, are similar in all three systems and agree reasonably with micelle-based NMR structures. When in the bilayer, the peptide increases the chain *gauche* population and area of adjacent lipids in the same binding leaflet, while it has the opposite effect for the nearby lipids of the other leaflet. These changes, which occur spontaneously to fill voids and defects, cause a decrease in the thickness of the membrane in the neighborhood of the peptide. They would be expected to promote positive curvature, as consistent with the formation of the convex bulge, or "nipple", in the initial stage of membrane fusion. An extension of the classical surfactant theory of Israelachvili based on shapes is proposed to introduce the concept of a "dynamically induced shape" of the membrane lipids by the peptide.



*Keywords:* viral fusion; hemagglutinin; fusion peptide; peptide–micelle interaction; molecular dynamics

## Introduction

The first stage of infection by a virus is penetration into the host cell. For this, the virus must cross the cell membrane of the host without disrupting it. The influenza virus executes this process in four steps: binding to cell surface receptors, endocytosis through clathrin-coated pits and vesicles, delivery to endosomes, and finally fusion with the endosomal membrane induced by the low pH of this compartment.[1] The infection process is driven by the homotrimer hemagglutinin (HA). Each monomer of HA is composed of two subunits: HA1, a globular receptor-binding subunit, and HA2, a fibrous subunit with 20 residue N-terminal fusion domain, or "fusion peptide", GLFGA-IAGFI-ENGWE-GMIDG. At high or normal pH, the fusion peptide is folded in the interior of HA and inaccessible to the surrounding solution. In response to low pH in the endosome, HA changes conformation and exposes its fusion peptides. The peptides then bind to the endosomal membrane, and the HA trimers cluster.[1,2] These initial events are thought to be followed by the bending of HA trimers to bring the viral and endosomal membranes into close proximity. The membranes would bulge out towards each other in regions denoted "nipples",[3] and then form the structure known as the stalk.[3–5] This is the hemifused state, where lipids of the outer leaflets of the two membranes mix. The fusion pore then

Present address: P. Lagüe, Département de biochimie et microbiologie, Faculté des Sciences et de Génie, CREFSIP, Université Laval, Que. Canada G1K 7P4.

Abbreviations used: DPC, dodecylphosphocholine; POPC, palmitoyl oleoyl phosphatidylcholine; POPG, palmitoyl oleoyl phosphatidylglycerol; HA, hemagglutinin; EPR, electron paramagnetic resonance; MD, molecular dynamics; SASA, solvent accessible surface area.

E-mail address of the corresponding author: patrick.lague@rsvs.ulaval.ca

0022-2836/$ - see front matter © 2005 Published by Elsevier Ltd.

forms in the center of the stalk and dilates, leading to mixing of lipids from the inner leaflets and, finally, to irreversible fusion.[1,2,6] It is proposed that the fusion peptides prime the target membrane for the energetically unfavorable high curvatures of fusion intermediates (nipple, stalk and pore) by increasing the membrane area and permeability,[7–8] and ordering the lipid chains and dehydrating the membrane surface.[9]

The fusion peptide segments of HA2 are of singular importance since they are the only parts of the virus directly in contact with the target membrane, and are essential for the fusion to occur. *In vivo*, the fusion peptide is part of HA and becomes exposed and inserts only at low pH. Synthetic variants of the fusion peptide (not attached to HA) also insert into lipid bilayers at both low and neutral pH.[6,10–12] Hemolysis and fusion of liposomes composed of palmitoyl oleoyl phosphatidylcholine (POPC) and palmitoyl oleoyl phosphatidylglycerol (POPG) (4:1) take place, though only at low pH.[11] The structure of the isolated fusion peptide associated with lipid bilayers has been recently determined at pH 7.4 (the non-fusogenic form) and pH 5 (fusogenic).[6,10] For this, the authors combined the information from high-resolution NMR structures determined in micelles and membrane depth estimated from electron paramagnetic resonance (EPR) experiments. The peptide has a kinked structure at both pHs, and is located at the lipid/water interface. A conformational change occurs in the peptide when the pH is lowered, triggering a deeper insertion into the membrane. The location of the peptide suggests points where the bilayer might be disrupted and fusion thereby promoted. Similar inferences have been drawn from a study on fusion peptide analogs.[13] Recent molecular dynamics (MD) simulations of the fusion peptide in bilayers[14,15] support these ideas; i.e. the peptide, located at the lipid/water interface, has two helices separated by a kink, and induces the thinning of the membrane[14,15] and lowers the lipid chain order parameters.[14]

Despite these advances, numerous issues remain unresolved. First, although there are indications that the fusion peptide has roughly the same secondary structure in micelles and bilayers,[6,10] subtle and potentially important differences may occur. For example, local peptide motions are sometimes more restricted in micelles than in bicelles,[16] while the mobility of transmembrane α-helices is approximately 30% higher in micelles than in bilayers.[17] The smaller size and curved shape of micelles can slightly alter peptide structures.[18] Hence, it is important to determine the nature and the origin of the small differences observed between micelles and bilayers, especially because micelles are increasingly used as model membranes in solution NMR.[19] Second, due to the dynamical nature of the system, it is difficult to study experimentally the impact of the fusion peptide on bilayers at a molecular level. A detailed description of changes in the neighboring lipids is essential for understanding peptide-induced fusion.

Here we address the preceding issues based on the results of MD simulations of the influenza HA fusion peptide associated with two different dodecylphosphocholine (DPC) micelles and with a POPC bilayer membrane. Four of the NMR models derived by Han *et al.*[10] were chosen as initial conditions of the peptide for trajectories. Details on the assembly of these 12 systems and other simulation issues are provided in Methods. The first part of the next section compares the peptide structure in the micelles with that of the bilayer, and with experiment. The second part considers the impact of the fusion peptide on the structure of the bilayer.

## Results and Discussion

### Comparison of micelle and bilayer systems

Four trajectories, denoted A–D, were initialized from four of the 20 NMR-based structures of the fusion peptide.[10] Unless otherwise noted, averages are over the last 2 ns of the 5 ns trajectories for the bilayer, and the last ns of the 2 ns trajectories of micelles containing 32 (denoted the 32mer) and 56 (the 56mer) DPC. The 56mer corresponds to the experimental aggregation number for DPC micelles, while the 32mer corresponds to the experimental aggregation number for DPC micelles with a bound peptide molecule.[20] The bilayers were composed of 123 POPC: 64 in the lower leaflet and 59 in the upper, peptide-containing, leaflet. The asymmetry in lipid number between the leaflets was fixed to accommodate the peptide without inducing either positive or negative curvature. Standard errors in the mean for each system were evaluated from averages over the four independent trajectories.

Figure 1 (top row, 32mer; middle row, 56mer; bottom row, bilayer) shows three different representations of the final trajectory frame from trajectory B. As expected for an amphipatic helix, the peptide resides in the lipid/water interface with its hydrophilic residues exposed to water and its hydrophobic residues in contact with the lipid hydrocarbon chains. Nevertheless, there are important differences evident in the first column of Figure 1: the N-terminal region of the peptide inserts deeply in the bilayer, while the entire peptide lies on the surface of the micelles. Consequently, hydrophobic residues are less exposed to the water molecules in the bilayer than in micelles. The top-down views in Figure 1 (middle column with peptide, and right column with peptide graphically removed) indicate that the peptide substantially distorts the 32mer, while it appears to conform more to the surface of the 56mer; the deep cleft in the bilayer occupied by the peptide is also evident. The following peptide properties are compared below: secondary structure, including the kink angle and hydrogen bond

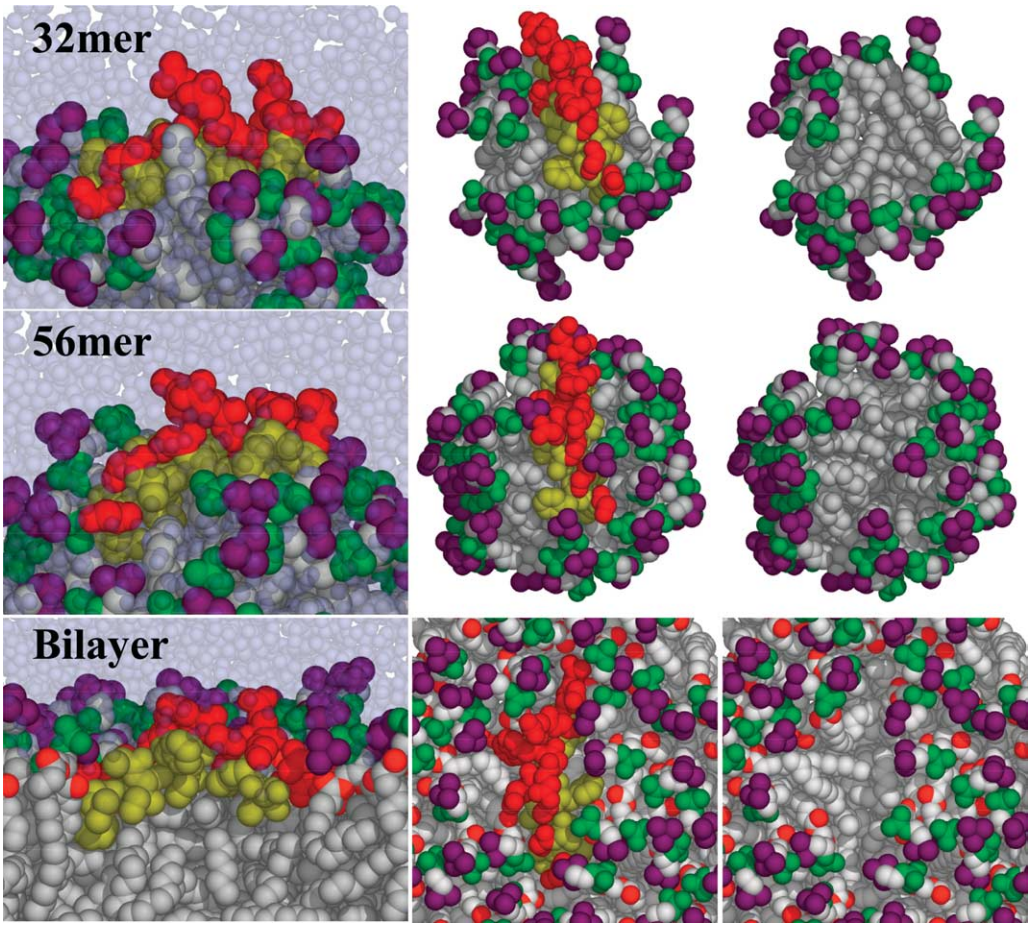


**Figure 1.** Different representations of the final frame from trajectory B of the fusion peptide in DPC micelles consisting of 32 lipids (top row), 56 lipids (middle row) and the POPC bilayer (bottom row). Water molecules are represented by transparent blue spheres (left column), lipids and peptides by opaque Van der Waals spheres (choline groups in purple and phosphate groups in green for the lipids; hydrophilic residues in red and hydrophobic residues in yellow for the peptides). Some lipids and water molecules have been removed from the bilayer picture of the left column to increase the visibility of the peptide in the first column. All water molecules are omitted in middle and right columns, and the fusion peptide is not shown in the right column.

patterns; solvent accessible surface area (SASA) and hydration; a detailed comparison with the NMR models, including root mean square difference (RMSD) and violations of experimental constraints.

### *Secondary structure*

As a starting point, the secondary structure was investigated with the DSSP software.[21] The first rows of Table 1 list the assignments for the peptide average structures from the simulations. In all cases a predominantly α-helical structure is disrupted by at least one residue in a hydrogen bonded turn. This motif of two helices separated by a kink is also found in the experimental structures (last rows in Table 1, and overlays in Figure 2), though the helical content is slightly lower. The simulated bilayer has a higher α-helical content than any micelle-based

**Table 1.** Secondary structure assignment for the fusion peptide for the simulated systems, and the four NMR models[10] used as initial conditions for these simulations

| Residue | 2 | 3 | 4 | 5 | 6 | 7 | 8 | 9 | 10 | 11 | 12 | 13 | 14 | 15 | 16 | 17 | 18 | 19 |
|---|---|---|---|---|---|---|---|---|---|---|---|---|---|---|---|---|---|---|
| Sequence | L | F | G | A | I | A | G | F | I | E | N | G | W | E | G | M | I | D |
| 32mer | H | H | H | H | H | H | H | H | H | H | H | T | H | H | H | H | H | T |
| 56mer | H | H | H | H | H | H | H | H | H | H | H | T | G | G | G | S | S | |
| Bilayer | H | H | H | H | H | H | H | H | H | H | T | H | H | H | H | H | H | H |
| Model 1 | H | H | H | H | H | H | H | H | H | T | T | T | T | H | H | H | H | |
| Model 19 | H | H | H | H | H | H | H | H | H | H | T | T | T | H | H | H | H | |
| Model 5 | H | H | H | H | H | H | H | H | T | T | T | T | T | H | H | H | H | T |
| Model 12 | H | H | H | H | H | H | H | H | H | T | T | T | T | H | H | H | H | |

H indicates a α-helix, T a hydrogen bonded turn, G a $3_{10}$-helix and S a bend. Missing entries denote none of the preceding structures.

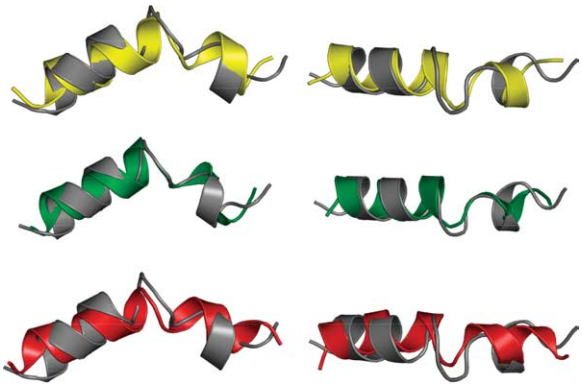

**Figure 2.** Overlays of the average structures from simulations (colored) with Model 5 (gray): 32mer (top row, yellow), 56mer (middle row, green) and bilayer (bottom row, red). The right column shows the top views of the pictures of the left column. Model 5 is from micelle NMR experiments.[10]

structure. This agrees with the experimental results of Han *et al.*,[10] who reported a slightly higher helical content in bilayers.

In order to determine the possible impact of the shape of the lipid aggregate on the peptide structure, the average angle between the two helices was calculated from the trajectories using the Chothia, Levitt, and Richardson algorithm.[22] From Table 2, the angle values in the 32mers and bilayers are similar and slightly higher than in the 56mers. These angles are generally greater than those of the initial conformers used for the simulations, which vary from 78° (Model 2) to 110° (Model 5). A difference in behavior between the two micelle systems may be at the origin of the slight angle difference (32mers are more distorted by the peptide) while a difference in peptide solvation may cause the small differences observed between 56mers and the bilayers.

Another observable related to the kink in the peptide is the hydrogen bond pattern that stabilizes it. The initial conformers were chosen according to the presence or absence of specific hydrogen bonds (Methods and Table 5). The hydrogen bonds involved are observed in 50% of the conformers determined by NMR[10] and are between the side-chain of N12 and the carbonyl of G8, and between the NH of W14 and the carbonyl of F9. The occupancies of these hydrogen bonds during the simulations are reported in Table 2. For the hydrogen bond between the side-chain of N12 and the carbonyl of G8, the occupancy is low (6–17%). The carbonyl of G8 is frequently (77–92%) hydrogen bonded with the amide of N12, thereby stabilizing the α-helix. The hydrogen bond between the amide of W14 and the carbonyl of F9 is of intermediate probability (51–75%), forming a hydrophobic pocket typical of the fusogenic conformers.[6,10] However, this hydrogen bond shows the greatest variation among the three systems and is less frequent in bilayer. Nuclear Overhauser effects (NOEs) observed experimentally[10] between backbone and side-chain of I10 and W14 are also observed in simulations, and these interactions are reflected by the presence of hydrogen bonds occurring between the carbonyl of I10 and different hydrogen atoms from the side-chain of W14, with very short lifetimes (2–20 ps).

### *Solvent accessible surface area and hydration*

As shown in Table 2, the total SASA of the peptide is approximately twice as high when it is micelle as opposed to the bilayer. The relative differences in hydrophobic surface exposure are even more pronounced. The micelle bound peptides are also more hydrated than those in the bilayer, as estimated by the average number of water molecules within 4.5 Å of each amino acid. The exposed hydrophobic surface area of the lipid chains is

**Table 2.** Assorted averages for the fusion peptide in two DPC micelles (32 and 56mers) and a POPC bilayer

| Property | 32mers | 56mers | Bilayer |
|---|---|---|---|
| Peptide bend angle (deg.) | 133 (4) | 114 (7) | 138 (3) |
| H-bond: N12 (side-chain)-G8 (carbonyl) (%) | 17 | 6 | 17 |
| H-bond: N12 (amide)-G8 (carbonyl) (%) | 92 | 77 | 88 |
| H-bond: W14 (amide)-F9(carbonyl) (%) | 75 | 60 | 51 |
| Peptide SASA: total (Å$^2$) | 967 (30) | 897 (48) | 483 (15) |
| Peptide SASA: hydrophobic (Å$^2$) | 96 (12) | 70 (9) | 24 (1) |
| Number of waters <4.5 Å | 8.2 (1.1) | 8.1 (1.1) | 6.4 (1.1) |
| Lipid SASA: hydrophobic/lipid chain (Å$^2$) | 7.3 (0.2) | 4.4 (0.1) | 4.4 (0.2) |
| Average RMSF (Å) | 1.34 (0.04) | 1.51 (0.04) | 1.62 (0.03) |
| Average RMSD (from PDB structures) (Å) | 2.56 (0.06) | 2.69 (0.04) | 2.98 (0.04) |
| NMR constraint violations | | | |
| Number of NOE constraint violations >1 Å | 2 | 3 | 4 |
| Number of angle constraint violations >10° | 8 | 11 | 9 |
| Number of spin-spin coupling constant violations >1 | 1 | 1 | 1 |

The root mean squared deviations (RMSD) and root mean squared fluctuations (RMSF) were calculated using all the backbone heavy atoms. The average number of water moleculess within 4.5 Å is expressed on a per amino acid basis. The cutoff for the spin–spin coupling constant violations is dimensionless. Standard errors evaluated from the averages over the four simulations for each system are included in parentheses.

substantially higher in the 32mer than in the bilayer, though this quantity is comparable for the 56mer and in the bilayer. These observations support the inference from Figure 1 that the peptide is more deeply complexed in the bilayer than in the micelles.

The root mean squared fluctuations, RMSF, from the trajectories (Table 2) indicate that the peptide is more flexible in the bilayer than in micelles. This flexibility is thereby correlated with burial in the lipid chains and anti-correlated with exposure to water. It is also consistent with the experimental observations of Andersson and Mäler[16] regarding the membrane peptide motilin in micelles and bicelles, and demonstrates a limitation of micelles as bilayer surrogates.

### *Comparison with NMR conformers*

The average and individual RMSD of the simulated peptide backbone with respect to the 20 different models of the original Protein Data Bank (PDB) entry[10] are listed in Tables 2 and 3, respectively. In each case, agreement with the experimental models is best for the 32mer and worst for the bilayer. This is to be expected because these models are derived from experimental NMR data using DPC micelles. The individual values vary from 1.97($\pm$0.07) Å for the 32mer structure against Model 5, to 3.39($\pm$0.07) Å for the bilayer structure against Model 2. The RMSD of the NMR models against themselves (final column of Table 3) range from 0.87 to 1.73 Å. Hence, the deviation of the simulated models from experiment is statistically significant, though relatively small. For all three systems, the lowest RMSD values are found against Model 5 while the highest are found against Model 2. This underscores the relative similarity of the simulated structures.

**Table 3.** RMSD (Å) for the backbone of the fusion peptide for the different simulated systems with respect to each of the NMR-based models

| PDB Model no. | System | | | Against other NMR models |
|---|---|---|---|---|
| | 32mers | 56mers | Bilayer | |
| 1 | 2.43 | 2.61 | 2.83 | 0.89 |
| 2 | 3.09 | 3.13 | 3.39 | 1.73 |
| 3 | 2.38 | 2.52 | 2.90 | 1.17 |
| 4 | 2.73 | 2.79 | 3.17 | 1.01 |
| 5 | 1.97 | 2.24 | 2.64 | 1.62 |
| 6 | 2.25 | 2.39 | 2.72 | 1.35 |
| 7 | 2.72 | 2.77 | 3.08 | 0.87 |
| 8 | 2.50 | 2.63 | 2.84 | 0.86 |
| 9 | 2.79 | 2.85 | 3.16 | 0.94 |
| 10 | 2.86 | 2.92 | 3.15 | 1.03 |
| 11 | 2.40 | 2.55 | 2.83 | 1.42 |
| 12 | 2.70 | 2.75 | 3.04 | 0.90 |
| 13 | 2.53 | 2.68 | 2.96 | 0.86 |
| 14 | 2.53 | 2.68 | 2.96 | 0.86 |
| 15 | 2.63 | 2.69 | 2.93 | 0.99 |
| 16 | 2.75 | 2.80 | 3.10 | 1.05 |
| 17 | 2.58 | 2.67 | 2.83 | 0.96 |
| 18 | 2.28 | 2.57 | 2.94 | 1.66 |
| 19 | 2.40 | 2.74 | 3.15 | 1.57 |
| 20 | 2.72 | 2.79 | 3.05 | 0.87 |

Standard errors range from 0.03 to 0.09. The final column lists the RMSD of each NMR model against the other 19.

The final entries in Table 2 summarize the discrepancies of the simulated peptides with the 149 NOE upper limit constraints and 52 dihedral angle constraints obtained from NMR measurements.[10] Time-average distances were evaluated from the trajectories as $\langle r^{-6}\rangle^{-1/6}$, where $r$ is the instantaneous distance between selected atoms, and compared to the upper limit constraints obtained from NMR measurements. The number of violations larger than 1 Å is reasonably small, with the lowest number for the peptide in 32mers and the largest in bilayers. The largest violations ($\approx$ 2 Å) occur between the amide of I18 and the $\gamma$2 protons of its side-chain for bilayers, and between the amides of N12 and W14 for the micelles.

Violations with dihedral constraints were evaluated from averages calculated directly from the simulations, and from the spin-spin $J$-coupling constants calculated from the following Karplus-type relations:[23,24]

$$^3J_{\mathrm{HN}\alpha}(\varphi) = 6.4\cos^2(\varphi - 60^\circ) - 1.4\cos(\varphi - 60^\circ) + 1.9 \quad (1)$$

$$^3J_{\mathrm{HN}\alpha}(\chi^1) = 9.5\cos^2(\chi^1 - 120^\circ) - 1.6\cos(\chi^1 - 120^\circ) + 1.8 \quad (2)$$

where the second equation applies for the β-methine proton in Ile. The number of angle constraint violations is lowest in 32mers and highest in the 56mers. The violations occur mostly with side-chain angles, with the $\chi^1$ of L2, F3 and I6, $\chi^{21}$ of I6 and I10, and $\chi^2$ of M17 the most frequent. All three systems show a single violation of the spin–spin coupling constraints. Overall, the agreement of simulation and experiment is good and is similar for the micelles and the bilayer.

## Impact of the peptide on bilayers

This section considers the change of the bilayer structure induced by the presence of the fusion peptide. First, an analysis of the position and orientation of the peptide in the bilayer is presented. The following lipid properties relative to peptide position are then described: lipid chain distributions; chain order parameters and *gauche* bond fractions; lipid chain length and area; headgroup orientation and the membrane thickness. Finally, the results are used to speculate on how the peptide induces curvature of the bilayer. Following conventions in the field,[3,4] the leaflet containing the peptide is denoted "*cis*", and the opposing leaflet is denoted "*trans*".

### *Position in the bilayer*

The position of the peptide in the bilayer has been previously estimated using a docking method.[6,10]

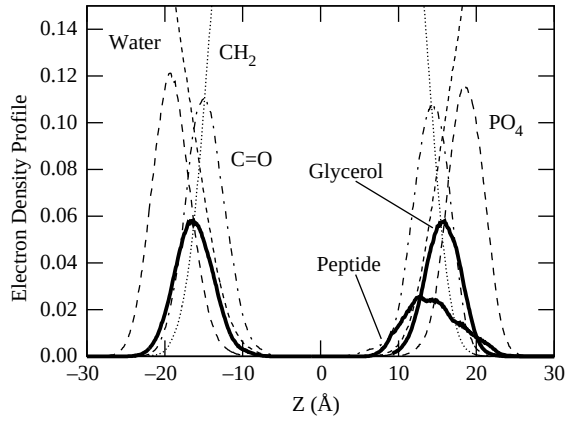


**Figure 3.** Average electron density profile of the main components of the fusion peptide-POPC bilayer systems. All atoms were recentered according to the center of mass of the chain terminal methyl groups to average the four trajectories consistently.

Molecular models were built from experimental NMR structures, and these models were fit in the bilayer using EPR data of (different-position) spin-labeled fusion peptides in bilayer, and a calibration curve obtained from spin-labeled lipids. The best fits place the $C^{\alpha}$ of N12 approximately at the same position of the lipid phosphate groups along the bilayer normal, $z \approx 19$ Å.[6,10] The peptide was placed in this position at the beginning of simulations (see Methods). The membrane thinned in the region near the peptide during equilibration, and the average equilibrium $z$ positions of the $C^{\alpha}$ of N12 and the adjacent lipid phosphate groups are 15.8($\pm$0.3) Å and 16.6($\pm$0.1) Å, respectively; i.e. both the peptide and the neighboring phosphate groups were pulled toward the center of the bilayer.

Figure 3 plots the electron density profiles of the peptide/bilayer systems. While fusion peptide is primarily located in the glycerol and carbonyl regions, the N-terminal extends to within a few Ångstroms from the bilayer center. The distributions of lipid components are similar to those in pure bilayers, because the number of lipids in the system is large, and the effect of the peptide is localized.

### *Orientation of the peptide in bilayer*

The orientation of the peptide in bilayers has been determined experimentally by polarized attenuated total reflection FTIR (ATR-FTIR) spectroscopy,[11] and by docking EPR data.[6,10] This orientation can be measured from a MD trajectory from the peptide order parameter $S_{ATR}$:[25–27]

$$S_{ATR} = \frac{1}{n}\sum_{i=1}^{n}\left(\frac{3\cos^2(\theta_i)-1}{2}\right) \qquad (3)$$

where $\theta_i$ is the angle between the amide I transition moment and the normal to the interface for the $i$th residue. Following Bernèche *et al.*,[26] it is assumed here that the transition moment is parallel to the C=O backbone carbonyl bond. As the experimental dicroic ratio has been measured at a frequency of 1650 $cm^{-1}$,[11] and because this frequency is correlated to α-helix protein secondary structure,[27] only the C=O bonds participating in the α-helical secondary structure were included in the calculations. $S_{ATR}$ for the first helix = $-0.13 \pm 0.01$ and $-0.11 \pm 0.01$ for the second (shorter) helix. The order parameters from simulation yield angles of 29° and 31° with the plane of the bilayer for the first and second helices, respectively. These are close to the 38° obtained from a fit to the experimental EPR data[6] and the 33° from polarized FTIR spectroscopy,[11] and are identical to the angle observed for the first helix from recent MD simulations.[14] The angle between the two helices calculated from the respective orientation of the two helices is 120°, which is similar to the value of 138($\pm$3)° determined here (Table 2). Given the accuracy of the different methods used experimentally and theoretically, the agreement is satisfactory.

### *Lipid distribution around the fusion peptide*

Recent work by Feller *et al.*[28] unveiled the ability of membrane proteins to organize lipid orientation through preferential interactions with polyunsaturated lipid chains. This is because the high flexibility of polyunsaturated chains allows them to adapt their conformations to the irregular surface of proteins more easily than saturated chains. Although oleoyl chains are monounsaturated, and thereby less flexible than the polyunsaturated chains, there is potential for preferential solvation of the fusion peptide. To explore this possibility the center of mass radial distribution of the oleoyl and palmitoyl chains around the peptide was evaluated for the initial 500 ps and 3–5 ns segments of the trajectories. Figure 4 (bottom) shows that a layer enriched in oleoyl chains adjacent to the peptide is followed by a layer enriched in palmitoyl chains for the bilayers from the last segments of the trajectories; the distribution at the beginning of the simulations is considerably more uniform (Figure 4, top). As the length of the present simulations is shorter than the axial rotation timescale of the lipids (25–50 ns), it is likely that the movements leading to the space-filling around the peptide arise predominantly from isomerization of the lipid chains.

### *Lipid order parameters and* gauche *bond fractions*

The average structure in the interior of the bilayer can be characterized by the magnitude of the deuterium order parameter, $S_{CD}$. "Order parameter" here will be taken to be synonymous with $|S_{CD}|$, and was calculated as:

$$|S_{CD}| = \left|\frac{1}{2}\langle 3\cos^2\theta - 1\rangle\right| \qquad (4)$$

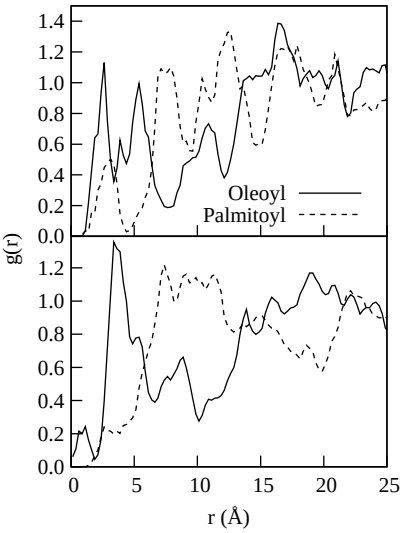


**Figure 4.** Two-dimensional radial distribution function, $g(r)$, based on the fusion peptide and lipid chain centers of mass for the beginning of the simulations (top) and from the last 2 ns of the trajectories (bottom) with oleoyl chains (continuous) and palmitoyl chains (broken). Only the lipids in the same leaflet as the peptide were included.

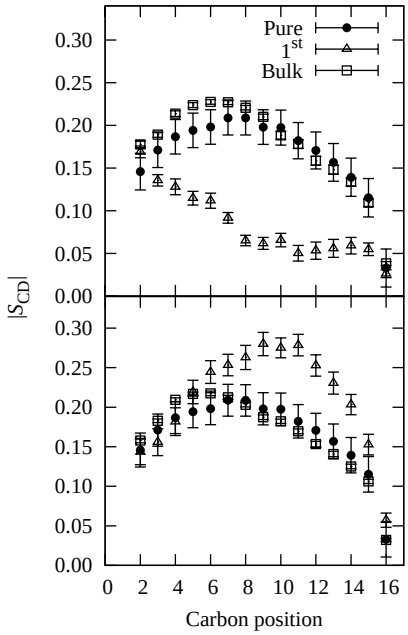


**Figure 5.** Deuterium order parameters, $S_{CD}$, for the palmitoyl chains for the different lipid categories, for the *cis* (peptide-containing) leaflet (top) and the opposing *trans* leaflet (bottom), and for a pure POPC bilayer (filled circles). The first neighbors are denoted by open triangles, and the bulk lipids in the peptide-containing bilayers by open squares. Standard errors are represented by the bars. The second neighbors are omitted for clarity.

where θ is the angle between the C–H bond vector and the bilayer normal and the brackets denote an average over time and over lipids of the same group and category. Lipids in the *cis* (peptide containing) and *trans* leaflets are considered separately, and further divided in three categories: first neighbors (those adjacent to the peptide), and second neighbors (those next to first neighbors), and bulk lipids (all others).

Calculated order parameters for the different lipid categories and those from a pure POPC trajectory simulated under the same conditions are compared in Figure 5 (for the palmitoyl chains) and Figure 6 (the oleoyl chains). For both palmitoyl and oleoyl chains, the values obtained for the bulk lipids and pure POPC are similar, indicating that the peptide does not perturb the lipids at these positions. In contrast, order parameters are substantially lower for first neighbors than for bulk lipids when in *cis* leaflet, and are higher for first neighbors in the *trans* leaflet. The order parameters of second neighbors (not shown in Figures 5 and 6 for clarity) are decreased for carbon positions 4–8 when in the *cis* leaflet; all other second neighbors have similar order parameters to bulk lipids. The oleoyl chains are somewhat less perturbed by the presence of the fusion peptide than the palmitoyl chains, possibly because their baseline level of disorder is relatively high.

A simple analysis indicates that the change in the order parameters in the vicinity of the peptide is predominantly caused by conformational adjustments, as opposed to lipid tilt or membrane bending. Specifically, Figure 7 compares *gauche* bond fractions for the first neighbors of the leaflets with those in a pure POPC bilayer. The results for the palmitoyl chains (Figure 7, top) indicate a systematically larger number of *gauche* bonds for the middle of the chain of the *cis* leaflet than for in

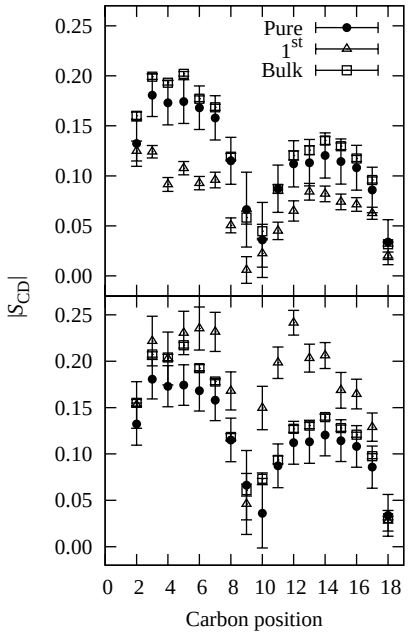


**Figure 6.** Deuterium order parameters for the oleoyl chains for the different lipid categories and leaflets, as for Figure 5.

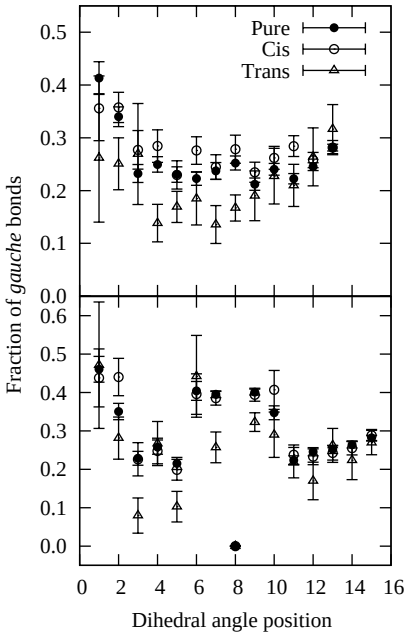


**Figure 7.** *Gauche* bond fractions for the first neighbors of the *cis* and *trans* leaflets and for pure a POPC bilayer for dihedral angle positions along palmitoyl (top) and oleoyl (bottom) chains. Standard errors are represented by the bars.

pure POPC bilayer, and a lower fraction for the middle of the chain of the *trans* leaflet. The fraction of *gauche* bonds is consistent with the reduction of the order parameter for chains in the *cis* leaflet, and the increase in the opposing leaflet. Consistent with the trends in the order parameters, the differences in *gauche* fractions are somewhat smaller for the oleoyl chains (Figure 7, bottom).

The differential effect observed here was also found in simulations of melittin, where a decrease in $|S_{CD}|$ for lipids in the same leaflet as the peptide[26,29] was coupled with increased order in the opposite leaflet.[26] Zemel *et al.*[30] obtained qualitatively similar results using a mean-field chain-packing theory for lipids and a peptide modeled as a cylinder. Vacarro *et al.*[14] noted a decrease in $|S_{CD}|$ for the lipids in the *cis* leaflet in their simulations, but did not report values for the *trans* leaflet. Other simulated results have been more varied, and system-dependent. A decrease in the order parameter was found for lipids in the neighborhood of Gramicidin S[31] and dermaseptin S3 and MB21.[32] An increase was observed for gramicidin A in a DMPC membrane.[33] In effect, peptides modulate the bilayer in different ways.

There is no significant deviation from the isomerization rates of lipids in pure POPC bilayer (results not shown), indicating that on average the internal chain dynamics is not perturbed by the presence of the peptide.

### *Lipid chain length and area*

Table 4 lists the chain end-to-end distances for the two chains and their positions in the bilayer relative to the peptide. First neighbors in *cis* leaflet are shortened while those in the *trans* leaflet are extended compared to the bulk lipids or the pure POPC bilayer. These results are again consistent with the change in order parameters and *gauche* fraction bonds, as the first neighbors in the peptide-containing leaflet are more curled, and the first neighbors in the opposite leaflet are more extended.

Next, the areas occupied by the lipid from the different positions were estimated as follows: (1) the lipid molecules were divided in different components, each component having the pre-determined volume specified by Armen *et al.*;[34] (2) the occupancy numbers of the different lipid components along the normal bilayer were calculated for the different lipid positions relative to the peptide; (3) the total lipid area for a given position $z$ along the bilayer normal is then deduced from the occupancy numbers and their respective component volumes:

$$A_z = \sum_{i}^{\text{nb of components}} \frac{n_i(z)V_i}{\Delta z} \qquad (5)$$

where $n_i(z)$ is the occupancy number of a given lipid component, $V_i$ is the volume related to this component and $\Delta z$ is the slice thickness; (4) the area occupied by a lipid is determined by the highest value of its area along the $z$-axis. This method yields accurate lipid area values and is independent of the nature of the lipid neighbors.

**Table 4.** Average distance between the beginning and the end of the chains, and lipid areas as function of lipid positions

| | | Distance between ends (Å) | | |
|---|---|---|---|---|
| Leaflet | Position | Palmitoyl | Oleoyl | Lipid area (Å$^2$) |
| *Cis* | 1$^{st}$ neigh. | 15.3 (0.1) | 15.6 (0.1) | 82.6 (3.7) |
| | 2nd neigh. | 15.8 (0.1) | 15.5 (0.1) | 71.6 (2.2) |
| | Bulk | 15.7 (0.1) | 16.1 (0.1) | 67.1 (1.6) |
| *Trans* | 1$^{st}$ neigh. | 16.7 (0.1) | 17.5 (0.1) | 60.4 (3.3) |
| | 2nd neigh. | 15.9 (0.1) | 17.0 (0.1) | 64.6 (2.6) |
| | Bulk | 15.7 (0.1) | 16.1 (0.1) | 66.2 (1.0) |
| Pure POPC | – | 15.6 (0.1) | 16.2 (0.1) | 65.7 (1.6) |

The results from a pure POPC bilayer are included for comparison purpose. Standard errors in parentheses.

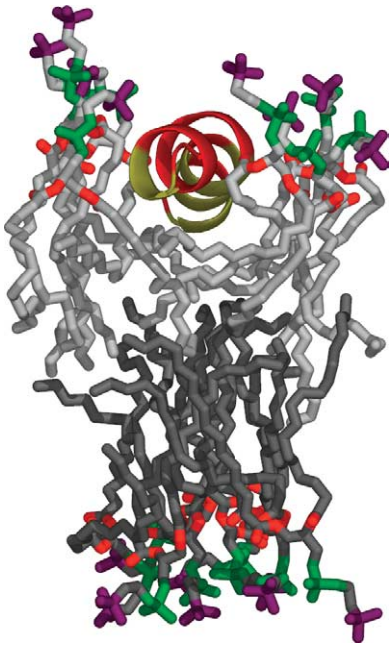

**Figure 8.** Packing of lipids around the fusion peptide from the 3.5 ns point of trajectory C.

The last column of Table 4 lists the lipid areas as function of the lipid categories in the peptide/bilayer system, and for the pure POPC bilayer. These results show again the first neighbor lipids are the most perturbed by the peptide presence in the bilayer, whereas the bulk lipids occupy an area about the same value as pure POPC lipids. The dramatic increase in lipid area of first neighbors of the top leaflet, with the increased *gauche* fractions and the lowering of the order parameters, is a clear indication that space-filling around the peptide arises from bending of the aliphatic chains of these lipids rather than from tilting the whole lipid. The first neighbors in the *trans* leaflet occupy a smaller area with a decreased *gauche* fraction, consistent with a higher order parameter. These adjustments are very evident in Figure 8. A systematic examination of other snapshots revealed a similar pattern. The lipid chains adjacent the peptide curl under the hydrophobic residues and those on the *trans* leaflet extend into the *cis* leaflet. In this sense, the chains of the *cis* leaflet are ordered, even though their $|S_{CD}|$ are lower than found in a pure POPC bilayer.

### *Membrane thickness and polar head orientation*

The average phosphate to phosphate distance between leaflets equaled 36.3($\pm$0.2) Å for the first neighbors, 35.8($\pm$0.3) Å for second neighbors and 38.3($\pm$0.3) Å for bulk, and 38.4($\pm$0.3) Å for pure POPC. Hence, there is a decrease of 2–2.5 Å in the thickness of the membrane in the neighborhood of the fusion peptide. Such thinning has been also observed from previous MD simulation studies,[14,15] and predicted by the mean-field theory of Zemel *et al*.[30]

In contrast, the polar head PN vector orientations in the bilayer with the peptide exhibit little dependence on position, and were similar to pure POPC. Similar behavior was observed in MD simulations of melittin.[26]

### *Membrane curvature induced by the fusion peptide*

Prior to actual fusion, the membrane locally adopts a large positive curvature when it bulges into the convex shape of the nipple. The stalk, which appears at the next stage of fusion, has both positive and negative (concave with respect to the outer surface) curvatures, though its net curvature is negative.[3] While the bilayers simulated here are too small to adopt the curvatures associated with the preceding intermediates, the propensity for curvature may be inferred from the present results. As quantified above and illustrated in Figure 8, the fusion peptide increases the conformational disorder and surface area in the *cis* leaflet, and decreases disorder and surface area in the *trans* leaflet. The likely consequence of these perturbations, sketched in Figure 9, is a propensity for positive curvature. Such a curvature would promote formation of the convex bulge, which is required in the early stage of fusion to overcome the considerable repulsion between two flat membranes.

The preceding inference draws from the classical surfactant theory of Israelachvili based on "shapes".[35] Specifically, this theory shows how the relative cross-sectional area of the polar headgroup and hydrophobic chains determines the propensity of a surfactant to adopt a particular phase, such as cubic, hexagonal, micelle or lamellar. The change in the local intrinsic curvature of the membrane proposed here is induced by the presence of the bound fusion peptide and, more importantly, by its effect on the dynamical chain order of the lipids in

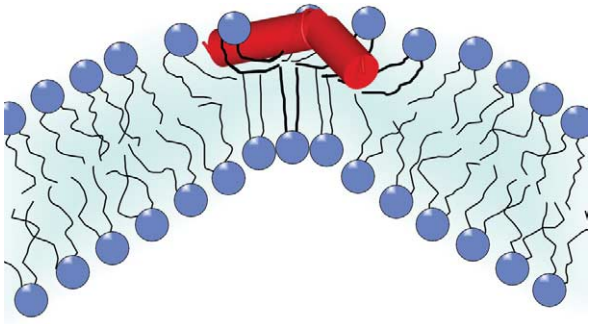

**Figure 9.** Schematic view of how the fusion peptide might prime the membrane for the early stages of fusion by inducing a local positive curvature from the differences in cross-sectional area and chain conformations of the two bilayer leaflets near the peptide. The net negative curvature associated with later stages of fusion is not considered here.

the *cis* and *trans* leaflets. These effects are not static. The resulting spatial arrangement of the peptide–lipid complex may, therefore, be considered an example of "dynamically induced shape". This concept recognizes that the bilayer membrane is a conformationally plastic and dynamical environment that reacts in a complex way to the presence of impurities.

Lastly, the hypothesis that the fusion peptide promotes negative curvature and thereby contributes to the stabilization of the stalk,[3,4] has not been considered in the study. Simulating systems with net-negative curvature, such as the fusion stalk, will require a substantially larger number of lipids, because surfaces with both negative and positive curvature must be accommodated. It is also likely that more peptides are required.

## Conclusion

The present work presents the results from MD simulations of the HA2 fusion peptide in micelles containing 32 and 56 DPC molecules, and in bilayers. The results are averaged over four independent trajectories (5 ns each for the bilayer and 2 ns each for the micelles) for each of the three systems. It was demonstrated that the conformation of the fusion peptide is similar when bound to either micelles or bilayers. This validates the use of micelles as an experimental surrogate for bilayers. As importantly, it demonstrates that the lipids are more plastic than the peptide; i.e. the peptide forces the lipids to adjust, not the other way round. However, micelles and bilayers respond to the peptide in different ways. In the former, the lipids can freely adjust their positions, and the micelle can change shape with little energy cost. The surface of a bilayer is less deformable than that of a micelle, and the lipids must adjust their conformations. The fusion peptide is also somewhat less flexible in micelles than in bilayers. This is likely a result of deeper burial in the bilayer leading to increased interaction with lipid chains and decreased hydration.

The differential nature of the conformational reorganization of the lipids around the membrane-bound fusion peptide is the central result of this study. As illustrated in Figure 8 and quantified by lipid chain order parameters, fraction of *gauche* bonds, and lipid cross-sectional areas, the configurations and positions of lipids in each leaflet shift differently to accommodate the peptide. Figure 9 sketches the proposed consequence: a local distortion of the chains and thinning of the bilayer that promote the positive curvature associated with early fusion. Longer timescale and lengthscale simulations with larger numbers of lipids and peptides will be required to refine these observations, and to investigate the net-negative curvature structures associated with later fusion events. Nevertheless, the present results strongly imply that the fusion peptide is a not simple membrane-anchor, and show how it may play an active role in altering the local structural properties of the bilayer.

The present dynamically induced shape hypothesis may be considered an extension of the classical surfactant theory of Israelachvili, where the shape of the lipids (specified by the ratio of the headgroup and chain cross-sectional areas) determines the phase. Here the fusion peptide changes the shape of neighboring lipids.

## Methods

### Simulation details

Simulations were performed with the program CHARMM[36] using the CHARMM27 all-atom potential energy parameter set[37] with TIP3P waters.[38,39] Electrostatic interactions were calculated *via* the Particle Mesh Ewald (PME) method,[40] using a sixth-order spline interpolation for the complementary function, with $\kappa = 0.34\ \text{Å}^{-1}$, and a fast-Fourier grid density $\approx 1\ \text{Å}^{-1}$. Cutoffs for the real space portion of the PME calculation and for the truncation of the Lennard-Jones interactions were 11 Å, with the latter smoothed *via* a switching function over the range of 8 to 11 Å. The long-range Lennard-Jones terms are taken into account with a pressure-based long-range correction (LRC) method.[41] Briefly, this LRC consists of an additional applied pressure tensor, which is periodically calculated from the difference of instantaneous pressures at the cutoff and a very long cutoff. Here, the selected cutoff is 11 Å, the very long cutoff is 30 Å, and the period between updates is 10 ps.

SHAKE[42] was used to constrain all covalent bonds involving hydrogen atoms. All simulations employed the leapfrog Verlet algorithm, and an integration step of 1 fs. Coordinates were saved every 0.5 ps. Non-bond and image lists were updated every 20 steps. Net translation and rotation of the systems were removed every 1000 steps. The thermostat coupling constant was 20,000 kcal ps$^2$ and the piston mass equaled 2500 amu. The following ensembles were used: NPT for micelle systems and NPAT for bilayer systems, where N, P, A and T denote particle number, pressure, surface area, and temperature, respectively. Finally, all simulations were carried out at 30 °C.

### Peptide configurations

The fusion peptide is composed of 20 amino acid residues: GLFGA-IAGFI-ENGWE-GMIDG. The starting configurations were picked from PDB entry 1IBN,[10] which contains 20 NMR structures of the peptide in DPC micelles at pH 5.0. Four models were chosen for their presence or not of some hydrogen bonds stabilizing the "kinked" structure. The criteria used to determine the presence of a hydrogen bond are a distance of less than 2.8 Å between the amide hydrogen and the carbonyl oxygen, and a O–H–N angle $>120°$.[43] These hydrogen bonds, observed experimentally in 50% of the structures, are between the side-chain of N12 and the carbonyl of G8, and between the NH of W14 and the carbonyl of F9. The four models (denoted here A, B, C, and D) and their respective particular hydrogen bond patterns are presented in Table 5.

**Table 5.** NMR models used as initial conditions for the trajectories, and their hydrogen bond patterns stabilizing the kink structure

| Trajectory | Model no. in PDB file | Side-chain N12–carbonyl G8 | Amide W14–carbonyl F9 |
|---|---|---|---|
| A | 1 | Yes | Yes |
| B | 19 | No | No |
| C | 5 | No | Yes |
| D | 12 | Yes | No |

Glu and Asp residues were unprotonated. The neutral glycine (GLYN) patch was used for the first residue, and the amidated C terminus (CT2) patch for the last. The GLYN patch was adapted from the CHARMM22 topology file for small model compounds, and no new atom type, functional group or parameters were required. It was necessary to add one angle and three dihedral terms to the CHARMM potential: NH2-CT2-C ($k_\theta = 52.0$, $\theta_0 = 108.0$), HC-NH2-CT2-C ($k_\chi = 0.110$, $n = 3$, $\delta = 0.0$), NH2-CT2-C-NH1 ($k_\chi = 0.500$, $n = 1$, $\delta = 0.0$), and O-C-CT2-NH2 ($k_\chi = 0.0$, $n = 1$, $\delta = 0.0$), where $k_\theta$, and $\theta_0$ are respectively the force constant and the equilibrium value for the angle, and $k_\chi$, $n$, and $\delta$ are the force constant, the multiplicity and the minimum geometry of the dihedral. The terms were added by assuming transferability from closely analogous terms, adopting CT2-CT2-C for the angle term, X-CT3-NH2-X, NH3-CT2-C-NH1 and NH1-C-CT2-NH1, and O-C-CT2-NH1 for dihedral terms.

### DPC micelles

This subsection outlines the assembly and equilibration of the four fusion peptide-DPC micelle systems (one for each initial structure). The assembly of these systems is derived from work described elsewhere.[44,45] Micelles of 32 and 56 molecules were chosen for simulations, the 56mers correspond to the experimental aggregation number for DPC micelles, while the 32mers correspond to the experimental aggregation number for DPC micelles with a bound peptide molecule.[20]

First, the peptide was put in place, the center of mass symmetrical according to $x$- and $y$-axis, and 11 Å away from the origin of the $z$-axis, the pocket of the peptide pointing toward the origin and the hydrophilic residues oriented outside of the sphere. Then, DPC molecule configurations were randomly picked from a Langevin Dynamics (LD) (timestep $\Delta t = 0.001$ ps, temperature $T = 30$ °C, collision frequency $\gamma = 5.0\ \text{ps}^{-1}$) of a single DPC, where the P and phosphoether O atoms were constrained and aligned along a radial vector. Configurations were rejected when the projection of the P and the terminal methyl group along the radial vector was less than 10 Å. DPC molecules were then translated, placing the P atom of each 18 Å from the origin and rotating the molecule to random points on a sphere, with DPC atoms at least 2 Å away from any peptide atoms. The final assembly was energy minimized with 50 steps of steepest descent (SD) followed by 500 steps of Adopted Basis Newton Raphson (ABNR), with the potential shifted to zero at 12 Å and a distance-dependent dielectric constant. For this minimization, the peptide atoms were constrained.

Each model was then inserted to a pre-equilibrated rhombic dodecahedron of 8085 water molecules, and water molecules whose O were within 2 Å of any DPC or peptide atoms were deleted. 18 $Cl^-$ and 21 $Na^+$ ions were added *via* random replacement of water molecules more than 6 Å away from any solute or previously placed ion. This number of ion pairs yields a salt concentration of approximately 0.150 mM, and the three more $Na^+$ neutralize the negative charges of the peptide.

Last, the four solvated systems (one for each peptide model) were minimized with 150 steps of SD and ABNR each. The systems were then simulated for 2 ns in periodic boundary conditions with a rhombic dodecahedron unit cell, and the data were collected only for the last ns. The peptides were constrained for the minimization and for the first 500 ps of the simulation. A 2 ns trajectory took about 500 h to produce on eight AMD 1.4 GHz Athlon processors interconnected with myrinet network cards.

### POPC bilayers

Again, four different systems were built, one for each initial structure. Each peptide was first put in place, at the position and orientation in bilayers suggested by the work of Han *et al.*,[10] i.e. the $C^\alpha$ of N12 at the average position of the lipid phosphate groups (about 19 Å from bilayer's center[46]), and an angle of 37° with the bilayer's plane for the first helix formed by residues 2 to 10. Next, the initial configuration of the bilayer around the peptide was constructed from pre-equilibrated and pre-hydrated POPC lipids as described,[26,33,47] with a cross-sectional area of 64 $Å^2$ per lipid.[34] The POPC bilayer consisted of 123 lipids (64 for the lower leaflet and 59 for the upper, where the peptide stands), and around 30 water molecules for each lipid. Then 10 $Cl^-$ and 13 $Na^+$ ions were added *via* random replacement of water molecules more than 6 Å away from any solute or previously placed ion.

The velocities were initialized at −70 °C, and the simulation was run for 50 ps with the temperature increased by 10 deg.C every 1 ps, up to 30 °C, using periodic boundary conditions with a tetrahedral unit cell. A harmonic constraint was applied the first 300 ps to prevent water penetration in the bilayer. The peptide was constrained for 1750 ps, then NOE restraints were applied on hydrogen bonds present in the initial structure and gradually removed over the next 300 ps. Coordinates were saved every 0.5 ps for the range of 3 ns to 5 ns for subsequent analysis. A 5 ns trajectory took about 1250 h to produce on eight AMD 1.4 GHz Athlon processors interconnected with myrinet network cards.

In order to verify if the asymmetry in lipid number between the upper and lower leaflets was correct, a 1.5 ns MD simulation using the $P2_1$ periodic boundary conditions[48] was started from the final frame of the simulation of structure A in the bilayer. The $P2_1$ periodic boundary conditions allow lipids to "flip" between the upper and lower leaflets. Over the last 1 ns of simulation using these conditions, the average number of lipids of the upper leaflet was $59.3 \pm 0.2$. This result supports the use of 59 lipids for the leaflet where the fusion peptide is located.

Finally, the pure POPC bilayer consisted of 128 lipids (64 in each leaflet), and 3657 water molecules. The initial configuration was constructed from pre-equilibrated and pre-hydrated lipids as described,[26,33,47] with a cross-sectional area of 64 $Å^2$ per lipid.[34] Velocities were initialized at −70 °C, and the simulation was run for 50 ps where the temperature was increased by 10 deg.C every 1 ps, up to 30 °C. After 1 ns of equilibration, a 1 ns production run at NPAT/LRC was carried out.

## Acknowledgements

We thank L. K. Tamm for sharing experimental NMR data, J. Zimmerberg and C.D. Weiss for valuable discussions, and R. M. Venable for technical advice. This study utilized the high-performance computational capabilities of the Biowulf PC/Linux cluster at the National Institutes of Health, Bethesda, MD. (http://biowulf.nih.gov). B.R. is supported by NIH grant GM-62342.

## References

1. Hernandez, L. D., Hoffman, L. R., Wolfsberg, T. G. & White, J. M. (1996). Virus-cell and cell–cell fusion. *Annu. Rev. Cell. Dev. Biol.* **12**, 627–661.
2. Gruenke, J. A., Armstrong, R. T., Newcomb, W. W., Brown, J. C. & White, J. M. (2002). New insights into the spring-loaded conformational change of influenza virus hemagglutinin. *J. Virol.* **76**, 4456–4466.
3. Kuzmin, P. I., Zimmerberg, J., Chizmadzkev, Y. A. & Cohen, F. A. (2001). A quantitative model for membrane fusion based on low-energy intermediates. *Proc. Natl Acad. Sci. USA*, **98**, 7235–7240.
4. Epand, R. M. (1998). Lipid polymorphism and protein–lipid interactions. *Biochim. Biophys. Acta*, **1376**, 353–368.
5. Gingell, D. & Gindberg, L. (1978). Problems in physical interpretation of membrane interaction and fusion. In *Membrane. Fusion* (Poste, G. & Nicholson, G. L., eds), pp. 791–833, Elsevier, Amsterdam.
6. Tamm, L. K. (2003). Hypothesis: spring-loaded boomerang mechanism of influenza hemagglutinin-mediated membrane fusion. *Biochim. Biophys. Acta*, **1614**, 14–23.
7. Longo, M. L., Waring, A. J. & Hammer, D. A. (1997). Interaction of the influenza hemagglutinin fusion peptide with lipid bilayers: area expansion and permeation. *Biophys. J.* **73**, 1430–1439.
8. Zhelev, D. V., Stoicheva, N., Scherrer, P. & Needham, D. (2001). Interaction of synthetic HA2 influenza fusion peptide analog with model membranes. *Biophys. J.* **81**, 285–304.
9. Gray, C., Tatulian, S. A., Wharton, S. A. & Tamm, L. K. (1996). Effect of the N-terminal glycine on the secondary structure, orientation and interaction of the influenza hemagglutinin fusion peptide with lipid bilayers. *Biophys. J.* **70**, 2275–2286.
10. Han, X., Bushweller, J. H., Cafiso, D. S. & Tamm, L. K. (2001). Membrane structure and fusion-triggering conformational change of the fusion domain from influenza hemagglutinin. *Nature Struct. Biol.* **8**, 715–720.
11. Han, X. & Tamm, L. K. (2000). A host-guest system to study structure-function relationship of membrane fusion peptides. *Proc. Natl Acad. Sci. USA*, **97**, 13097–13102.
12. Han, X. & Tamm, L. K. (2000). pH-dependent self-association of influenza hemagglutinin fusion peptides in lipid bilayers. *J. Mol. Biol.* **304**, 953–965.
13. Hsu, C.-H., Wu, S.-H., Chang, D.-K. & Chen, C. (2002). Structural characterizations of fusion peptide analogs of influenza virus hemagglutinin. *J. Biol. Chem.* **277**, 22725–22733.
14. Vaccaro, L., Cross, K. J., Kleinjung, J., Strauss, S. K., Thomas, D. J., Wharton, S. A. *et al*. (2005). Plasticity of influenza haemagglutinin fusion peptides and their interaction with lipid bilayers. *Biophys. J.* **88**, 25–36.
15. Huang, Q., Chen, C.-L. & Herrmann, A. (2004). Bilayer conformation of fusion peptide of influenza virus hemagglutinin: a molecular dynamics simulation study. *Biophys. J.* **87**, 14–22.
16. Andersson, A. & Mäler, L. (2002). NMR solution structure and dynamics of motilin in isotropic phospholipid bicellar solution. *J. Biomol. NMR*, **24**, 103–112.
17. Patargias, G., Bond, P. J., Deol, S. S. & Sansom, M. S. P. (2005). Molecular dynamics simulations of GlpF in a micelle vs in a bilayer: conformational dynamics of a membrane protein as a fonction of environment. *J. Phys. Chem. B*, **109**, 575–582.
18. Chou, J. J., Kaufman, J. D., Stahl, S. J., Wingfield, P. T. & Bax, A. (2002). Micelle-induced curvature in a water-insoluble HIV-1 Env peptide revealed by NMR dipolar coupling measurement in a stretched polyacrylamide gel. *J. Am. Chem. Soc.* **124**, 2450–2451.
19. Kallick, D. A., Tessmer, M. R., Watts, C. R. & Li, C.-Y. (1995). The use of dodecylphosphocholine micelles in solution NMR. *J. Magn. Reson. B*, **109**, 60–65.
20. Lauterwein, J., Bösch, C., Brown, L. R. & Wüthrich, K. (1979). Physicochemical studies of the protein-lipid interactions in melittin-containing micelles. *Biochim. Biophys. Acta*, **556**, 244–264.
21. Kabsch, W. & Sander, S. (1983). Dictionary of protein secondary structure: pattern recognition of hydrogen-bonded and geometrical features. *Biopolymers*, **22**, 2577–2637.
22. Chotia, C., Levitt, M. & Richardson, D. (1981). Helix to helix packing in proteins. *J. Mol. Biol.* **145**, 215–250.
23. Pardi, A., Billeter, M. & Wuthrich, K. (1984). Calibration of the angular dependence of the amide proton-$C^{\alpha}$ proton coupling constants, $^{3}J_{HN\alpha}$, in a globular protein. Use of $^{3}J_{HNa}$ for identification of helical secondary structure. *J. Mol. Biol.* **180**, 741–751.
24. DeMarco, A., Llinas, M. & Wuthrich, K. (1978). Analysis of the 1H-NMR spectra of ferrichrome peptides. I. The non-amide protons. *Biopolymers*, **17**, 617–636.
25. Axelsen, P. H., Kaufman, B. K., McElhaney, R. N. & Lewis, R. N. A. H. (1995). The infrared dichroism of transmembrane helical polypeptides. *Biophys. J.* **69**, 2770–2781.
26. Bernèche, S., Nina, M. & Roux, B. (1998). Molecular dynamics simulation of Melittin in a dimyristoylphosphatidylcholine bilayer membrane. *Biophys. J.* **75**, 1603–1618.
27. Tamm, L. K. & Tatulian, S. A. (1997). Infrared spectroscopy of proteins and peptides in lipid bilayers. *Quart. Rev. Biophys.* **30**, 365–429.
28. Feller, S. E., Gawrisch, K. & Woolf, T. B. (2003). Rhodopsin exhibits a preference for salvation by polyunsaturated docosohexaenoic acid. *J. Am. Chem. Soc.* **125**, 4434–4435.
29. Bachar, M. & Becker, O. M. (2000). Protein-induced membrane disorder: a molecular dynamics study of mellitin in a dipalmitoylphosphatidylcholine bilayer. *Biophys. J.* **78**, 1359–1375.
30. Zemel, A., Ben-Shaul, A. & May, S. (2004). Membrane perturbation induced by interfacially adsorbed peptides. *Biophys. J.* **86**, 3607–3619.
31. Mihailescu, D. & Smith, J. C. (2000). Atomic detail peptide-membrane interactions: molecular dynamics simulation of gramicidin S in a DMPC bilayer. *Biophys. J.* **78**, 1718–1730.

32. Shepherd, C. M., Vogel, H. J. & Tieleman, D. P. (2003). Interactions of the designed antimicrobial peptide MB21 and truncated dermaseptin S3 with lipid bilayers: molecular dynamics simulations. *Biochem. J.* **370**, 233–243.
33. Woolf, T. B. & Roux, B. (1996). Structure, energetics, and dynamics of lipid-protein interactions: a molecular dynamics study of the gramicidin A channel in a DMPC bilayer. *Proteins: Struct. Funct. Genet.* **24**, 92–114.
34. Armen, R. S., Uitto, O. D. & Feller, S. E. (1998). Phospholipid component volumes: determination and application to bilayer structure calculations. *Biophys. J.* **75**, 734–744.
35. Israelachvili, J., Marcelja, S. & Horn, M. G. (1980). Physical principles of membrane organization. *Quart. Rev. Biophys.* **13**, 121–200.
36. Brooks, B. R., Bruccoleri, R. E., Olafson, B. D., States, D. J., Swaminathan, S. & Karplus, M. (1983). CHARMM: a program for macromolecular energy, minimization, and dynamics calculations. *J. Comp. Chem.* **4**, 187–217.
37. Feller, S. E. & MacKerell, A. D., Jr (2000). improved empirical potential energy function for molecular simulations of phospholipids. *J. Phys. Chem. B*, **104**, 7510–7515.
38. Jorgensen, W. L., Chandrasekhar, J., Madura, J. D., Impey, R. W. & Klein, M. L. (1983). Comparison of simple potential functions for simulating liquid water. *J. Chem. Phys.* **79**, 926–935.
39. Durell, S. R., Brooks, B. R. & Ben-Naim, A. (1994). Solvent-induced forces between two hydrophilic groups. *J. Phys. Chem.* **98**, 2198–2202.
40. Darden, Y. D., York, D. & Pedersen, L. (1993). Particle mesh ewald: an Nlog(N) method for ewald sums in large systems. *J. Chem. Phys.* **98**, 10089–10092.
41. Lagüe, P., Pastor, R. W. & Brooks, B. R. (2004). Pressure-based long-range correction for Lennard-Jones interactions in molecular dynamics simulations: application to alkanes and interfaces. *J. Phys. Chem. B*, **108**, 363–368.
42. Ryckaert, W. E., Ciccotti, G. & Berendsen, H. J. C. (1977). Numerical integration of the Cartesian equations of motion of a system with constraints: molecular dynamics of *n*-alkanes. *J. Comp. Chem.* **23**, 327–341.
43. Ravishanker, G., Vijaykumar, S. & Beveridge, D. (1994). STRIPS: an algorithm for generating two-dimensional hydrogen-bond topology diagrams for proteins. In *Modeling the Hydrogen Bond*, American Chemical Society, Washington, DC pp. 209–219.
44. Dixon, A. M., Venable, R. M., Pastor, R. W. & Bull, T. E. (2002). Micelle-bound conformation of a hairpin-forming peptide: combined NMR and molecular dynamics study. *Biopolymers*, **65**, 284–298.
45. Bogusz, S., Venable, R. M. & Pastor, R. W. (2000). Molecular dynamics simulations of octyl glucoside micelles: structural properties. *J. Phys. Chem. B*, **104**, 5462–5470.
46. Nagle, J. F. & Tristram-Nagle, S. (2000). Structure of lipid bilayers. *Biochim. Biophys. Acta*, **1469**, 159–195.
47. Allen, T., Andersen, O. S. & Roux, B. (2003). Structure of Gramicidin A in a lipid bilayer environment determined using molecular dynamics simulations and solid-state NMR data. *J. Am. Chem. Soc.* **125**, 9868–9877.
48. Dolan, E. A., Venable, R. M., Pastor, R. W. & Brooks, B. R. (2002). Simulations of membranes and other interfacial systems using $P2_1$ and Pc periodic boundary conditions. *Biophys. J.* **82**, 2317–2325.


***Edited by G. von Heijne***

*(Received 25 August 2005; received in revised form 7 October 2005; accepted 12 October 2005)*